All-Optical Control of an Individual Resonance in a Silicon Microresonator

Y. Henry Wen, Onur Kuzucu, Moti Fridman, Alexander L. Gaeta, Lian-Wee Luo, and Michal Lipson

Phys. Rev. Lett. **108**, 223907 — Published 1 June 2012

DOI: 10.1103/PhysRevLett.108.223907

All-Optical Control of an Individual Resonance in a Silicon Micro-Resonator

Y. Henry Wen,* Onur Kuzucu,† Moti Fridman, and Alexander L. Gaeta‡
School of Applied & Engineering Physics, Cornell University, Ithaca, NY 14853, USA

Lian-Wee Luo and Michal Lipson‡
School of Electrical & Computer Engineering, Cornell University, Ithaca, NY 14853, USA

We experimentally demonstrate selective control of the Q and transmission of an individual resonance of an optical micro-cavity by optically controlling its intra-cavity loss via inverse Raman scattering. A strongly over-coupled resonance is brought into critical coupling with continuous tuning of the on-resonance transmission by > 9 dB and reduction of the intrinsic Q factor by more than a factor of five. Adjacent resonances experience minimal disturbance and can be selectively controlled by tuning the control beam to the appropriate control resonance. These dynamics are analogous to Zeno effects observed in decoherence-driven atomic ensembles and two-level systems.

PACS numbers: 42.82.Et, 03.65.Xp, 42.65.Pc

On-chip micro-cavities have attracted significant interest for their ability to confine and manipulate light on a compact, scalable platform [1]. Such micro-resonators have been applied to modulators [2, 3], routers [4], optical delays [5, 6], detectors [7] and multiple-wavelength sources [8] for on-chip optical signal processing as well as probes and sensors for opto-fluidic manipulation [9], biochemical sensing [10, 11] and frequency metrology [12, 13]. Recent work on cavity-atom interactions offers the promise of ultra-small optical clocks and on-chip quantum optics [14–17].

Active modulation of on-chip optical cavities is typically achieved via a refractive index shift through free-carrier effects or the Kerr-nonlinearity [2, 4]. However the broadband nature of such index-shifts alters all of the resonance wavelengths and does not permit control of individual frequency channels of the cavity. This limits its full functionality as a multi-channel router and limits access to other important cavity parameters such as cavity Q, linewidth and on-resonance transmission, which are important for both active operation and post-fabrication fine-tuning of the cavity properties [18].

Recently, it was proposed [19] that these previously unaccessible functionalities can be achieved through all-optical control of a narrowband loss in the cavity at the signal wavelength by stimulating Raman loss through the inverse Raman scattering (IRS) process. In silicon, IRS produces a 105-GHz-wide (1-nm) spectral loss at the anti-Stokes wavelength which is blue-detuned by 15.6 THz with respect to the control beam. For a typical micro-resonator, this stimulated Raman loss (SRL) is spectrally wider than the cavity linewidth but narrower than the free spectral range (FSR), allowing it to alter a single resonance and leaving the adjacent resonances undisturbed. This resonant interaction enhances the coupling of the signal into the cavity making it far more efficient than a direct absorption switch. Furthermore, the coupled signal light continues to circulate in the ring cavity and can be re-routed with an adjoining drop waveguide [20]. Precision control of optical loss in optical cavities has also attracted recent interest for fundamental studies of light-matter interactions as coherent perfect absorption and time-reversed lasing in a fabry-perot cavity [23]. Additionally, optical resonators provide an optical analog for the quantum Zeno and anti-Zeno effects wherein the transition between two photonic states can be inhibited or enhanced through decoherence (*i.e.* optical loss) of the second state [21, 22].

Here we pres ent experimental demonstration of selective control of the intra-cavity loss of individual resonances of an optical cavity. The on-resonance transmission is reduced by 87%, and the Q_i is continuously tuned from 82,130 to 15,812 with a 13 pJ control pulse. This is achieved without shifting the resonance wavelength and with minimal disturbance to adjacent resonances. Adjacent signal resonances are controlled with similar efficiencies by tuning the control pulse to the adjacent control resonance. These observations are consistent with the predictions of coupled-mode theory for a loss-modulated cavity which confirms the resonant nature of the effect [19]. Lastly, we observe anti-Zeno- and Zeno-like dynamics in the response of the coupling of the waveguide and cavity modes to optical decoherence.

A ring resonator coupled to a single bus waveguide [Fig. 1(c)] has coupling region modeled by a coupling matrix given in Fig. 1(d), with field coupling-rate of $r = i\sqrt{1-t^2}$ and a field transmittance t, which is close to unity for a weakly coupled cavity. The on-resonance transmission at the through-port is given by,

$$T_{\mathrm{N}}(\lambda_{\mathrm{res}}) = \left[\frac{t-\alpha}{1-\alpha t}\right]^2, \tag{1}$$

where $\alpha(\lambda) = e^{-a_i(\lambda)L/2}$ is the round-trip field transmission of a ring cavity of circumference L, and $a_i(\lambda)$ is

* yhw2@cornell.edu
† Currently at Aselsan Inc., MGEO Tesisleri, Cankiri Yolu 7. Km Akyurt, Ankara 06750, Turkey
‡ Also at The Kavli Institute at Cornell for Nanoscale Science, Cornell University, Ithaca, NY 14853, USA

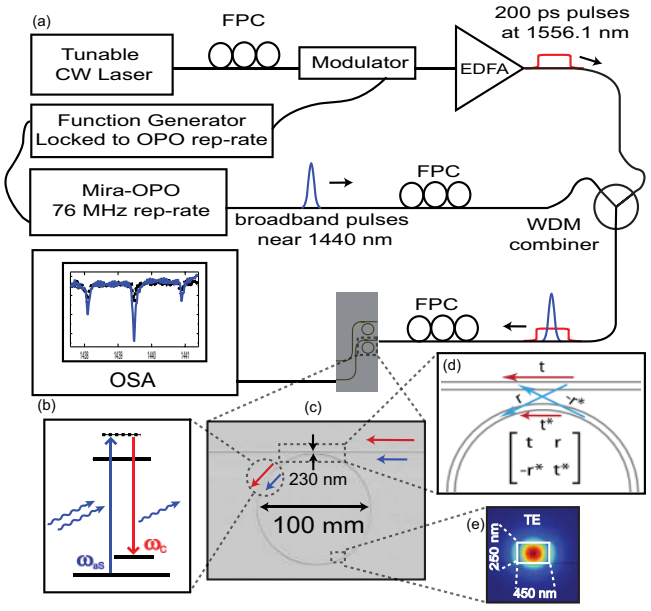

FIG. 1. (a) Schematic for all-optical control of a single resonance. 200 ps control pulses at 1556.1 nm are generated at the rep-rate of the optical parametric amplifier (OPO) which generates the broadband signal pulses near 1440 nm. The low power signal pulse does not cause nonlinear effects. The two pulses are combined and synchronized in time and injected into the silicon waveguide using a free-space objective. The through-port transmission is coupled out using a lens-tipped fiber and characterized by an optical spectrum analyzer with resolution of 0.01 nm. (b) Energy level diagram of IRS, (c) SEM image of ring-resonator, (d) Model of the coupling region using the scattering matrix formalism (e) simulation of TE mode cross-section.

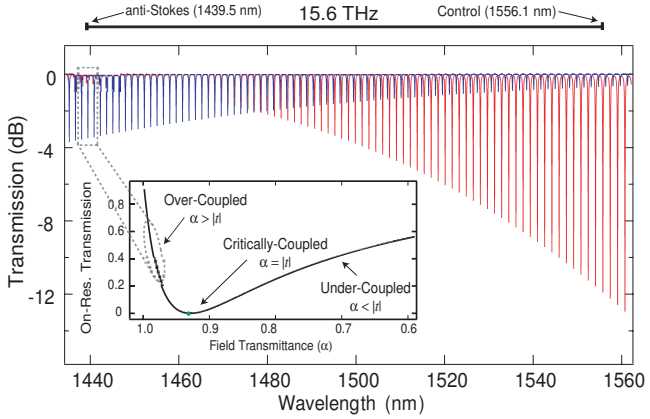

FIG. 2. Theoretical transmission of the TE (red) and TM (blue) modes across the relevant spectral range. Control (TE at 1556.1 nm) is near critical-coupling, anti-Stokes signal (TM at 1439.5 nm) is in strongly over-coupled. The two are separated by exactly Ω_R of silicon and are both resonant with the cavity. (Inset) Through-port transmission for a cavity as a function of the intra-cavity field transmission.

the intrinsic loss coefficient [19, 27]. The related Q factors provide an equivalent analysis of the system where $Q_{i,l} = \lambda/(a_{i,l}(\lambda) \cdot FSR \cdot R_{ring})$, FSR is the free-spectral-range and R_{ring} is the ring radius. We define the loaded loss coefficient $a_l(\lambda) = a_i(\lambda) - 2 \cdot ln(t)/L$, where the out-coupling is included as a loss process in the cavity. The on-resonance transmission in terms of the Q factors is $T_{\mathrm{N}}(\lambda_{\mathrm{res}}) = (1 - 2Q_l/Q_i)^2$. However, the $a(\lambda)$-t picture is the more natural basis with which to analyze the performance of the system since $a(\lambda)$ and t correspond directly to the controllable parameters of intra-cavity loss and coupling gap, respectively.

Figure 2 (inset) plots Eq. (1) as a function of α for t = 0.93 and shows that the transmission is most sensitive for values of α in the over-coupled regime, where the round-trip intra-cavity loss is less than the waveguide-cavity coupling-rate (i.e. $\alpha(\lambda) < |t|$). Without the control beam, only the linear loss contributes to the loss coefficient (i.e. $a(\lambda) = a_L$). The control beam stimulates Raman loss $a_R(\lambda, I)$ and generates several undesirable broadband nonlinear effects. Degenerate two-photon absorption (D-TPA) of the control grows quadratically with control power and generates free-carriers which causes free-carrier absorption (FCA). Non-degenerate TPA from control plus anti-Stokes photons adds to broadband loss of the signal, which grows linearly with control power. These two losses are represented as a lumped broadband loss $a_{NL}(I, I^2)$ such that $a(\lambda, I) = a_L + a_R(\lambda, I) + a_{NL}(I, I^2)$, where $I = \mathcal{F}_{eff} \cdot E_c/(\pi \cdot \tau_c \cdot A_{eff})$ is the intra-cavity intensity, $\mathcal{F}_{eff}$ is the effective finesse at the control wavelength, E_c is the control pulse energy, τ_c is the control pulse width and A_{eff} is the effective mode area of the waveguide. D-TPA of the signal is negligible due to the low signal powers in use. The broadband nonlinear losses and the associated refractive effects become a limiting process on the overall control efficiency and wavelength selectivity.

Inverse Raman scattering is a stimulated stokes scattering process wherein an anti-Stokes photon is scattered into a pump photon and the energy difference is deposited as an optical phonon in the material. Previously measured IRS in silicon nanowaveguides is consistent with the known Raman gain coefficient of $g_{\mathrm{R}} = 7$ cm/GW at the control wavelength 1550 nm [28]. The SRL near the anti-Stokes frequency ω_a is given by,

$$a_{\mathrm{R}}(\omega, I) = \frac{g_{\mathrm{R}} \Gamma_{\mathrm{R}}^2}{(\omega - \omega_a)^2 + \Gamma_{\mathrm{R}}^2} I, \qquad (2)$$

where $\Gamma_{\mathrm{R}} = 105$ GHz is the Raman loss linewidth for silicon. The FSR is chosen to be an integer fraction of Ω_R=15.6 THz such that the transverse electric (TE) control beam at 1556.1 nm and the transverse magnetic (TM) anti-Stokes signal beam at 1439.5 nm are simultaneously resonant with the ring. Figure 2 shows the theoretical transmission spectra of the TE (red) and TM (blue) modes and the spectral placement of the control and signal.

Simulations reveal that the cross-sectional dimensions of TE mode at 1439 nm is 15% shorter and 20%

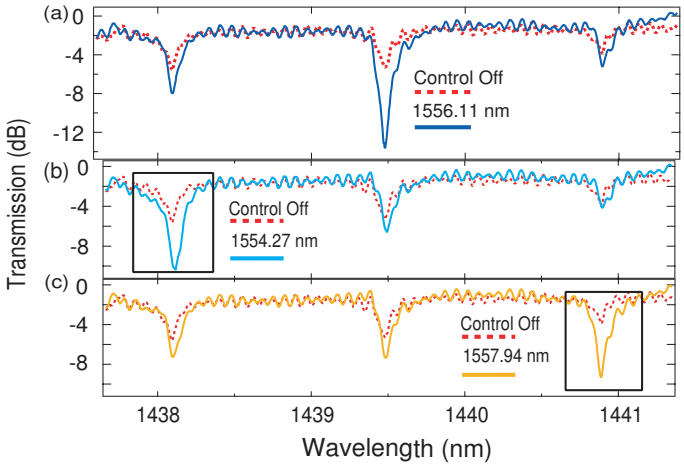

FIG. 3. Through-port spectra of three resonances near the anti-Stokes wavelength (TM) as the control pulse (TE) is tuned to the corresponding control resonances. The control pulses have an energy of 13 pJ. (a) Control: 1556.1 nm, anti-Stokes: 1439.54 nm; (b) Control: 1554.27 nm, anti-Stokes: 1437.97 nm; (c) Control: 1557.94 nm, anti-Stokes: 1441.11 nm

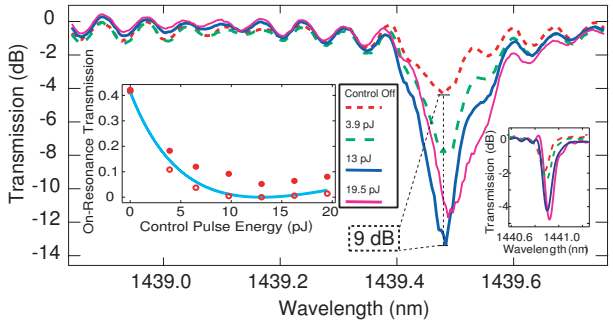

FIG. 4. Transmission of the anti-Stokes signal resonance (1439.5 nm, TM) with increasing control pulse energy (1556.1 nm, TE). (left inset) Comparison of the on-resonance transmission (solid dots) with Eq. (1) (blue line) and with a full-spectrum coupled-mode model (circles). (right inset) Response of adjacent resonance to increasing control pulse energy.

narrower than that of the TE mode at 1556 nm. This mode size difference leads to a significant difference in coupling rates for the control and signal. Using the more delocalized TM mode for the shorter anti-Stokes wavelength alleviates this difference for the disparate wavelengths. The Raman interaction in silicon is also stronger for orthogonally polarized control and signal beams. For waveguides fabricated on a wafer grown in the [001] direction and traveling in the [110] direction, the Raman interaction for TE-TM or TM-TE control-signal combination is enhanced by a factor of 3 over the TE-TE combination. In a circular ring cavity the control and signal fields sample all 2π of lattice directions which reduces the enhancement to a factor of 1.5 for the TE-TM combination over the TE-TE combination [29, 30]. This suggests that the Raman interaction can be increased by using racetrack cavities that extend the portions of waveguide which prefer the TE-TM combination.

The ring-resonators are fabricated on a 250-nm SOI wafer with 3 μm of buried oxide using standard CMOS fabrication processes. The rings have a radius of 50 μm, and are coupled to a straight waveguide separated by a gap of 230 nm. All waveguides have cross-section of 450-nm wide by 250-nm tall and have an effective mode area $A_{eff} = 0.25\ \mu m^2$. The anti-Stokes wavelength the field coupling rate is estimated to be $r = 0.55$ ($t = 0.83$) with an intrinsic loss of $a_L = 10.77$ dB/cm, which results in cavity resonances with an intrinsic $Q_i = 82{,}130$ but a loaded $Q_l = 12{,}613$. The large linear loss is due to the delocalized nature of the TM polarized mode and the large field coupling rate achieves initial over-coupling for the signal resonance. The control pulses are 200 ps which is close to the lifetime of the cavity. This reduces the effective finesse ($\mathcal{F}_{eff}$) from the steady-state value of 63 to 36. The optical transmission of the cavity was characterized using a low-power broadband pulse near the anti-Stokes wavelength (Fig. 1).

Figure 3 shows the narrowband SRL acting on single resonances. The affected resonance is exactly 15.6 THz blue-shifted from the control wavelength. The adjacent signal resonances can likewise be controlled by tuning the control wavelength to an adjacent control resonance such that the anti-Stokes loss shifts to the corresponding signal resonance [Figs. 3(b) and 3(c)]. This indicates that Raman loss is the dominant process affecting the resonances. The non-anti-Stokes resonances are not affected by the Raman loss, however the broadband TPA and FCA loss does result in modulation of their transmission by 1-2 dB for a 13-pJ control pulse. The contribution of the nonlinear losses to the system is further discussed in Fig. 5. A micro-resonator with flat dispersion can have 100's of doubly resonant pairs [12].

From Fig. 3 alone it is not conclusive whether the modulation is due to loss-induced resonant coupling, as we claim, or to SRL of the signal in the straight waveguide. Figure 4 shows the power dependance of the central resonance. The on-resonance transmission drops sharply from -4.3 dB to -13.3 dB (blue) for 13-pJ control pulse, equal to 4.7% transmission and >87% switching contrast. For control pulses greater than 13 pJ, the anti-Stokes transmission increases (purple, 19.5 pJ control pulse) indicating that the modulation cannot be due to direct absorption of the signal. Rather, the increase in transmission is consistent with a resonant cavity as described by Eq. (1) (Fig. 4 left inset). This is further confirmed by the continued decrease in transmission of the adjacent resonance (Fig. 4 right inset) and by the broadened linewidths of both resonances. Both observations indicate that the spectra for 19.5 pJ control pulse corresponds to greater loss, and hence greater power, inside the cavity. The signal loss due

to SRL in the straight waveguide is less than 0.1 dB. An off-resonant measurement of the Raman absorption at the anti-Stokes frequency in the straight waveguide reveals 0.25 dB of loss for a 20-pJ control pulse, but the loss is much less for resonant control and signal since the signal experiences Raman absorption for only 5% of the entire length of the straight waveguide.

Additionally, the linewidth, and therefore the Q, can be continuously tuned with increasing control energy. Figure 5 shows the single resonance intra-cavity loss and Q extracted from the resonance linewidth and extinction [31]. The initial Q_l is 6.5 times smaller than the initial Q_i of the cavity, but should be exactly 2 for a critically-coupled cavity. This ratio drops to 2.3 for a 13-pJ control pulse, indicating that the cavity is tuned close to critical coupling. For a 19.5 pJ control pulse, the Q_i decreases by a factor of 5.19, from 82,130 to 15,1812. Correspondingly, the intra-cavity loss increases by 45.2 dB/cm. Comparing the intra-cavity loss of the anti-Stokes resonance (Fig. 5, blue circle) with that of an adjacent resonance (green diamond) indicates that TPA and FCA contributes 16% (7.24 dB/cm) of the total loss of the anti-Stokes cavity, the other 84% (38.0 dB/cm) is due to Raman loss. TPA and FCA makes an appreciable contribution at high control powers due to its quadratic growth with control intensity. The sub-linear increase of the intra-cavity loss with the control pulse energy is consistent with broadband TPA and FCA reducing the Q factors for the control wavelength. The nonlinear losses measured from the adjacent resonance corresponds to a 45% decrease in both Q_l and $\mathcal{F}_{eff}$ at the control wavelength, in agreement with theoretical predictions (Fig. 5).

In the current scheme the passive signal transmission can be increased to greater than -0.2 dB (95%) by using a more over-coupled cavity. Routing applications require a drop waveguide to couple out the signal from the cavity where it would be advantageous to use an initially critically-coupled cavity and use the loss to push the cavity into under-coupled regime as described in [19]. The under-coupled regime allows complete isolation of the bus and drop waveguide in the on-state, which is not possible for the over-coupled cavity. For high-Q cavities (Q_l > 200,000), signal routing can be achieved with <0.1 signal loss (>97% transmission) for picojoule control energies. Selective routing of single channels dramatically increases the degrees-of-freedom and data density of the system. Networks of such devices with multiplicative degrees-of-freedom can easily be envisioned [32].

The dynamics shown here are also the optical analogue of Zeno effects observed in decoherence-driven atomic ensembles and quantum two-level systems where the natural evolution of the system is strongly perturbed by frequent measurement or decoherence on the upper state [22, 24]. This relation has been well established and is a current topic investigation by several groups [15, 21, 25]. In atomic systems [22, 24] measurement-induced decoherence enhances (anti-Zeno) the transition between two states for infrequent measurement and inhibits (Zeno) the transition for more frequent measurement. Here, the mode of the bus waveguide and the resonant mode of the cavity at the anti-Stokes wavelength represent the two photonic states, and the stimulated Raman absorption of anti-Stokes photons constitutes the measurements of the "upper" cavity state by coupling it to the phonon bath of the waveguide. The strength of the induced decoherence is directly (inversely) proportional to the frequency of (delay between) the loss events. For control pulses below 13 pJ, the cavity experiences anti-Zeno enhancement of the photonic transition but for higher control energies the cavity experiences Zeno inhibition of the transition. The current scheme provides a robust and sensitive platform for exploring the effects of loss on the thermodynamics of classical and quantum photonic states.

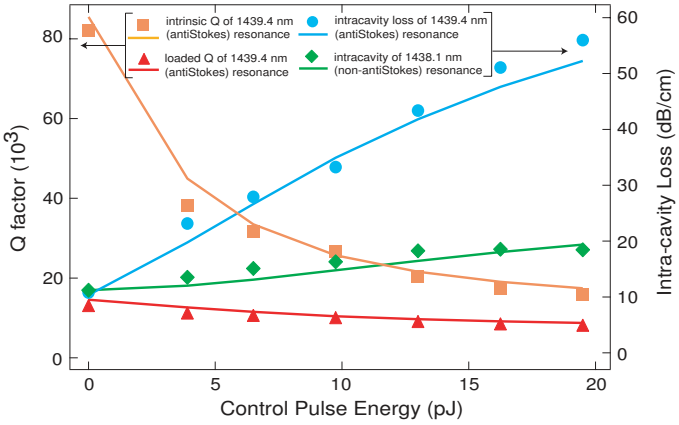

FIG. 5. Experimentally extracted values of the cavity loaded Q_l and intrinsic Q_i factors for the anti-Stokes resonance and intra-cavity loss for the anti-Stokes resonance and an adjacent resonance. A control pulse of 13 pJ corresponds to the condition closest to critical-coupling. Comparison of the intra-cavity loss of the two resonances reveals the contribution of TPA and FCA to loss in the system.

Stimulated Raman loss in silicon allows the manipulation of single cavity resonances in silicon micro-resonators. This system enables on-chip optical micro-cavities to achieve their full potential as multi-channel all-optical routers on a monolithic, CMOS compatible platform. This dramatically increases the degrees-of-freedom for design of both hardware and software for on-chip optical processing. Finally, it also demonstrates the universality of the effects of decoherence on resonant systems and their usefulness in controlling the system's dynamics.

The authors would like to acknowledge Y. Okawachi, A. Farsi, A. Griffith and G. Kurizki for insightful discussion and the Defense Advanced Research Projects Agency (DARPA) for supporting this work under the Zeno-based Opto-Electronics program.

[1] K. J. Vahala, Nature **424,** 839 (2003).
[2] V. R. Almeida *et al.*, Nature **431,** 1081 (2004).
[3] K. Nozaki *et al.*, Nature Photon. **317,** 783 (2007).
[4] B. G. Lee *et al.*, IEEE Photon. Tech. Lett.**20,** 767 (1998).
[5] J. Cardenas *et al.*, Opt. Express **18**, 26525 (2010).
[6] F. Xia *et al.*, Nat. Photon **1**, 65 (2007).
[7] Q. Fang *et al.*, Opt. Express **18**, 13510 (2010).
[8] M. A. Foster *et al.*, Opt. Express **19**, 14233 (2011).
[9] S. Mandal *et al.*, Nano. Lett. **10**, 99 (2010).
[10] A. M. Armani *et al.*, Nature **317,** 783 (2007).
[11] J. Zhu *et al.*, Nature Photon. **4**, 46 (2010).
[12] Y. Okawachi *et al.*, Opt. Lett **36**, 3398 (2011).
[13] T. J. Kippenberg *et al.*, Science **332**, 555 (2011).
[14] T. Aoki *et al.*, Phys. Rev. Lett. **102**, 083601 (2009).
[15] Y.-P. Huang and Prem Kumar, Phys. Rev. Lett **108**, 030502 (2012).
[16] S. Spillane *et al.*, Phys. Rev. A **71**, 013817 (2005).
[17] O'Brien *et al.*, Nat. Photon. **3**, 687 (2009).
[18] B. E. Little and Sai T. Chu *et al.*, IEEE Photon. Tech. Lett. **12**, 636 (2000).
[19] Y. H. Wen *et al.*, Opt. Lett. **36**, 1413 (2011).
[20] B. E. Little *et al.*, IEEE Photon. Tech. Lett. **10**, 816 (1998).
[21] B. C. Jacobs and J. D. Franson, Phys. Rev. A **79**, 063830 (2009).
[22] N. Erez *et al.*, Nature **452**, 724 (2008).
[23] W. Wan *et al.*, Science **331**, 889 (2011).
[24] M. C. Fischer *et. al.*, Phys. Rev. Lett **87**, 040402 (2001)
[25] J. Bernu *et. al.*, Phys. Rev. Lett **101**, 180402 (2008).
[26] L. Zhou and Le-Man Kuang, Phys. Rev. A **82**, 042113 (2010).
[27] A. Yariv IEEE Phot. Tech. Lett., **14**, 483 (2002)
[28] D. R. Solli, P. Koonath, and B. Jalali, Phys. Rev. A **79**, 053853 (2009).
[29] D. Dimitropoulos *et al.*, Opt. Lett. **28**, 1954 (2011).
[30] T. K. Liang and H. K. Tsang, Appl. Phys. Lett., **85**, 3343 (2003).
[31] L.-W. Luo *et al.*, Opt. Express **19**, 6284 (2011).
[32] S. Maniptruni *et al.*, Opt. Express **18**, 16858 (2010).
[33] H. Rong *et al.*, Nat. Photon., **1**, 232 (2007).